Available online at www.sciencedirect.com
SCIENCE DIRECT®
Inorganica Chimica Acta 355 (2003) 103–115
Inorganica Chimica Acta
www.elsevier.com/locate/ica

Comparison of (triphenylphosphine)ruthenium complexes containing the 2,2′:6′,2″-terpyridine (trpy) and 4,4′,4″-tri-*t*-butyl-2,2′:6′,2″-terpyridine (trpy*) ligands

Susan B. Billings [a], Michael T. Mock [a], Kevin Wiacek [a], Melinda B. Turner [a], W. Scott Kassel [a], Kenneth J. Takeuchi [b], Arnold L. Rheingold [c], Walter J. Boyko [a,*], Carol A. Bessel [a,*]

[a] *Department of Chemistry, Villanova University, 800 Lancaster Avenue, Villanova, PA 19085, USA*
[b] *Department of Chemistry, State University of New York at Buffalo, Buffalo, NY 14214, USA*
[c] *Department of Chemistry and Biochemistry, University of Delaware, Delaware, DE 19716, USA*

Received 22 January 2003; accepted 3 May 2003

Abstract

A comparison of (triphenylphosphine)ruthenium(II) complexes containing the 2,2′:6′,2″-terpyridine (trpy) and 4,4′,4″-tri-*t*-butyl-2,2′:6′,2″-terpyridine (trpy*) ligands was conducted. Electronic spectra and electrochemical data readily differentiated the *trans*- and *cis*-[$RuCl_2$(trpy or trpy*)(PPh_3)] complexes. ^1H, ^{13}C and ^{31}P NMR assignments were made for each of the isomers as well as the *trans*-[RuCl(trpy*)(PPh_3)$_2$](PF_6) complex. Notably, the ^{31}P chemical shift differences between the *trans*- and *cis*-[$RuCl_2$(trpy*)(PPh_3)] complexes were not dramatic and the ^1H NMR spectra were found to be the best way for determining the position of the triphenylphosphine ligand relative to the terpyridyl ligand. X-ray crystal structure analyses confirmed the structures of the *cis*-[$RuCl_2$(trpy*)(PPh_3)] and *trans*-[RuCl(trpy*)(PPh_3)$_2$]PF_6 complexes. Similar π-stacking interactions occurred between the phenyl rings and the trpy* ligand in both complexes.

Keywords: Ruthenium; NMR spectroscopy; Crystal structures; Terpyridine complexes

1. Introduction

The 2,2′:6′,2″-terpyridine (trpy) ligand has been widely studied as a chelating agent due to its chemical stability [1]. Several families of complexes containing substituted-trpy ligands have demonstrated unusual redox properties [2–4] and subsequently some of the families have been studied as stoichiometric and/or catalytic oxidants [5] as well as molecular recognition agents [6]. Additionally, the photochemistry and photophysics of some complexes containing substituted-trpy ligands remain a current interest, especially when contrasted with 2,2′-bipyridine (bpy)-containing ruthenium complexes [7–11].

While new synthetic procedures have considerably reduced the high cost associated with the synthesis of the trpy ligand [12], a number of synthetically modified trpy analogues have been developed to improve the ligand yield, the ligand chelating ability, and the specific electrochemical and/or spectroscopic properties of the transition metal complexes which incorporated these ligands [2–11,13–17]. The 4,4′,4″-tri-alkyl-2,2′:6′,2″-terpyridine ligands remain some of the most easily synthesized and purified of the substituted-trpy analogues [18].

Ben Hadda and Le Bozec [19,20] have reported the coordination of 4,4′,4″-tri-*t*-butyl-2,2′:6′,2″-terpyridine (trpy*) and 4,4′-di-*t*-butyl-2,2′-bipyridine (bpy*) in complexes of the form [Ru(bpy or bpy*)(trpy*)X]$^{n+}$ (where X = Cl^- or $CF_3SO_3^-$ and $n = 1$ or X = H_2O and

* Corresponding authors. Tel.: +1-610-519 4867 (W.J. Boyko), +1-610-519 4876 (C.A. Bessel); fax: +1-610-519 7167.
E-mail addresses: walter.boyko@villanova.edu (W.J. Boyko), carol.bessel@villanova.edu (C.A. Bessel).

0020-1693/03/$ - see front matter © 2003 Elsevier B.V. All rights reserved.
doi:10.1016/S0020-1693(03)00300-1

$n = 2$) or $Ru(bpy^*)_2Cl_2$. Le Bozec and coworkers [21] have also reported the results of thermal and photochemical isomerization studies which converted *trans*-$[RuCl_2(trpy^*)(Y)]$ to *cis*-$[RuCl_2(trpy^*)(Y)]$ (where Y = CO, PPh_3, PMe_3, PMePh, $P(OPh)_3$ or $P(OMe)_3$). In the latter publication, the authors used cyclic voltammetry to monitor the relative amounts of both the *trans*- and *cis*-$[RuCl_2(trpy^*)(Y)]$ products. The introduction of the bulky *t*-butyl substituent on the trpy ligand was observed to increase the solubilities of the (trpy*)ruthenium complexes in non-polar solvents relative to the parent (trpy)ruthenium complexes. The *t*-butyl substituents were also observed to donate electron density to the metal center and reduce the redox potentials of the resultant trpy* complexes relative to their trpy analogues.

Our group is interested in sterically large ligands and their effect on the properties of transition metal complexes [22–24]. We report here a more detailed comparison of the *trans*- and *cis*-$[RuCl_2(trpy^*)(PPh_3)]$ complexes with their trpy analogues using electronic spectroscopy, electrochemistry and ^1H, ^{13}C and ^{31}P NMR spectroscopies. The electronic and ^{13}C NMR spectroscopies of the $[RuCl_2(trpy^*)(PPh_3)]$ isomers have not been previously reported. We have also noted significant changes in the ^1H and ^{31}P NMR spectra for the *trans*-$[RuCl_2(trpy^*)(PPh_3)]$ isomer on aging; these changes have not been previously reported. Additionally, we report the X-ray structural analysis of the *cis*-$[RuCl_2(trpy^*)(PPh_3)]$ complex. To the best of our knowledge, this is the first time a crystal structure of the *cis*-geometry has been reported for (chloro)(phosphine)ruthenium complexes. Finally, we report the crystal structure of *trans*-$[RuCl(trpy^*)(PPh_3)_2](PF_6)$ and its comparison with similar *trans*-di(phosphine)(trpy)ruthenium complexes.

2. Experimental

2.1. Physical measurements

Elemental analyses were conducted by Atlantic Microlabs, Norcross, GA. Electronic spectra were measured with a Cary 1G Diode Array UV–Vis spectrophotometer. Cyclic voltammetry was conducted with a Bioanalytical Systems (BAS) 50 W potentiostat. Electrochemical measurements were conducted using a standard three-electrode cell arrangement. A saturated sodium chloride calomel (SSCE) reference electrode, a platinum wire auxiliary electrode and a platinum working electrode (Bioanalytical Systems) were used. The working electrode was polished with 0.5 μm alumina (Buehler Ltd. or Bioanalytical Systems) for 30 s, then sonicated in distilled water and rinsed with methanol rinse just prior to use. No *IR* corrections were made and all measurements were conducted at room temperature using 0.1 M tetrabutylammonium tetrafluoroborate (TBAB) in CH_2Cl_2 or CH_3CN as the electrolyte solution. The $E_{1/2}$ values for ferrocene at +0.40 V in CH_3CN or +0.50 V in CH_2Cl_2 were used as an internal standard.

^1H, ^{13}C and ^{31}P NMR spectra were recorded with a Varian 300 MHz Fourier Transform spectrometer in deuterated methylene chloride (CD_2Cl_2). ^1H NMR spectra were obtained at 299.9 MHz and referenced to tetramethylsilane. ^{13}C NMR spectra were obtained at 75.4 MHz and referenced to CD_2Cl_2. Proton–proton COSY and carbon–hydrogen HETCOR were run with standard Varian-supplied pulse sequences to confirm assignments. NMR spectral assignments for quaternary carbons were confirmed using the ChemWindow3 C-13 NMR module computer application [25].

The single-crystal X-ray diffraction experiments were performed on a Siemens P4/CCD diffractometer. Systematic absences uniquely defined the space group for both crystal structures and the choice of the space groups resulted in chemically reasonable structures that remained stable over the course of structural refinements. The structures were solved using direct methods and subsequent difference Fourier syntheses. Final structure refinements were made using full-matrix, least-squares procedures. All non-hydrogen atoms were refined with anisotropic displacement parameters. All hydrogen atoms were calculated in idealized positions. All software used in the structure determination and sources of the scattering factors were contained in the SHELXTL (5.10) program library [26].

2.2. Materials and preparations

Reagents were obtained from Aldrich Chemical Co. and used as received. The trpy* ligand was prepared according to slight variations in the literature procedures described by Rosevear and Sasse [18] and Ben Hadda and Le Bozec [19]. Preparations of $RuCl_3(trpy^*)$ (**1**), *trans*-$[RuCl_2(trpy^*)(PPh_3)]$ (**2**) and *cis*-$[RuCl_2(trpy^*)(PPh_3)]$ (**3**) have been previously reported [21]. The following are variations of literature procedures. All syntheses were carried out under N_2(g), unless otherwise noted.

2.2.1. *trans*-$[RuCl_2(trpy^*)(PPh_3)]$ (**2**)

A 1.01 g (1.66 mmol) of **1** and 0.650 g (2.48 mmol) triphenylphosphine (PPh_3) were mixed in 300 ml CH_2Cl_2 and outgassed with N_2(g). Triethylamine (15 ml) was added and the solution was heated to reflux for 1.5 h during which time the solution became purple. The solvent was removed using a rotary evaporator and the product was redissolved in a minimal amount of CH_2Cl_2 before passing down an alumina column. The column was eluted with CH_2Cl_2. The initial purple band was

collected, reduced in volume and then dripped into stirring hexanes. The purple solid was collected by vacuum filtration, washed with a minimal amount of hexanes, and air-dried. Often the product contained a small amount of impurity and so column chromatography was repeated a second time. Yield: 0.711 g (0.85 mmol), 51%. Anal. Calc. for $RuC_{45}H_{50}Cl_2PN_3$: C, 64.64; H, 6.04. Found: C, 64.52; H, 6.12%.

2.2.2. *cis*-[*RuCl*$_2$(*trpy**)(*PPh*$_3$)] (**3**)

A 0.0560 g sample (0.0669 mmol) of **2** was dissolved in 50 ml CH_2Cl_2 and refluxed by heating under a 120-W spotlight for 24 h. During this time, the color of the solution changed from purple to reddish-violet. The solid was reduced in volume and dripped into stirring diethyl ether. The product was vacuum-filtered, washed with a minimal amount of diethyl ether, and air-dried. Yield: 0.0356 g (0.0428 mmol), 64%. Elemental analysis was not performed as X-ray structural data were available (vide infra).

2.2.3. *trans*-[*RuCl*(*trpy**)(*PPh*$_3$)$_2$]*PF*$_6$ (**4**)

A 0.500 g (0.821 mmol) sample of **1** was mixed with 1.08 g (4.11 mmol) of triphenylphosphine along with 150 ml methylene chloride and 12.5 g of zinc amalgam. The reaction was heated to reflux for 24 h and then irradiated under a spotlight for 18 h. After the reaction was completed, the mixture was filtered to remove the zinc amalgam and the solution was reduced to dryness using a rotary evaporator. A solution of 30 ml of ethanol and 45 ml of water was added to dissolve the filtrate before a solution of 3.5 g NH_4PF_6 dissolved in a minimum amount of water was added, to cause the ruthenium complex to precipitate. The crude precipitate was collected by vacuum filtration, washed with a minimum amount of water, and air-dried. This product was purified on an alumina column using a CH_2Cl_2/CH_3OH eluent (90:10, v/v). The major orange band was reduced in volume on a rotary evaporator, dripped into stirring hexanes, and vacuum-filtered. The pure product was washed with a minimal amount of hexanes and air-dried. Yield: 0.674 g (0.558 mmol), 68%. Anal. Calc. for $RuP_3ClN_3C_{63}H_{65}F_6$: C, 62.66; H, 5.39. Found: C, 62.37; H, 5.57%.

3. Results and discussion

3.1. Synthesis

Scheme 1 represents the synthesis of complexes **2**–**4** (where the tridentate, N-donor ligand on the meridional plane is trpy*; see Scheme 2). The synthesis is initiated by combining complex **1** with PPh_3 and a reducing agent, NEt_3, to form complex **2**. Irradiation of a solution of **2** isomerizes the ruthenium geometry and produces **3**. The combination of **3** with excess PPh_3 produces the cationic species **4** which is precipitated after metathesis with PF_6^-. Complex **4** has not previously been reported.

3.2. Electronic spectroscopy

The electronic spectra of the ruthenium complexes **2**–**4** as well as their trpy analogues are reported in Table 1. Electronic spectra have not previously been reported for the (trpy*)ruthenium complexes. The absorbances in the UV region have been assigned to intraligand $\pi \rightarrow \pi^*$ transitions within both the trpy* ligand and the phenyl groups of the triphenylphosphine ligand(s) [23,24,27,28].

In the visible region, the lower energy absorption bands have been assigned to metal-to-ligand charge transfer (MLCT) transitions in analogy to other ruthenium(trpy) complexes [24,27,28]. The differences in the electronic spectra of the *trans*- and *cis*-[$RuCl_2$(L)(PPh_3)] (where L = trpy or trpy*) complexes are significant. The lowest energy absorption bands are assigned as manifolds of transitions which are predominantly Ru(dπ) $\rightarrow$ trpy*(π^*) in character. In the trpy complexes, the λ_{max} value of the lowest energy MLCT band in the *cis*-[$RuCl_2$(L)(PPh_3)] isomer (**3′**) is approximately 18 nm lower in wavelength than that for the corresponding *trans*-[$RuCl_2$(L)(PPh_3)] isomer (**2′**) [27]. In the trpy* complexes, this shift in wavelength for the two isomers is exactly the same, i.e., the MLCT band of **3** is 18 nm lower in wavelength than that of complex **2**. The shifts to higher energy and the more positive Ru(III/II) potentials of the *cis*-isomers are consistent with stabilization of the dπ levels in the *cis*-isomer when compared to the *trans*-isomer [27].

The addition of a second triphenylphosphine ligand to **3** and the consequent change from a neutral to a positively charged molecule results in a shift of the MLCT bands (again assigned to Ru(dπ) $\rightarrow$ trpy*(π^*) transitions) to higher energies. The shift from *cis*-[$RuCl_2$(L)(PPh_3)] to *trans*-[$RuCl$(L)(PPh_3)$_2$]$^+$ is evident in a decrease of the λ_{max} of 58 nm for the trpy complexes and 51 nm for the trpy* complexes.

Interestingly, a comparison of the trpy*-containing complexes **2** and **3** with the trpy-containing complexes **2′** and **3′** shows that the λ_{max} of the MLCT bands of the trpy* complexes are 7 nm lower in wavelength than those of the trpy complexes. These small shifts to lower wavelength are consistent with the greater electron-donating character of the *t*-butyl groups present on trpy* and are also evident in the electrochemical data (vide infra). The $E_{1/2}$ values of the trpy* complexes (**2** and **3**) are 40 mV less than the corresponding trpy complexes (**2′** and **3′**). The slightly higher energies of the MLCT bands observed for the trpy* complexes suggest that π^*-orbitals of the trpy* ligand increase the energy gap and stabilize the ruthenium(II) state.

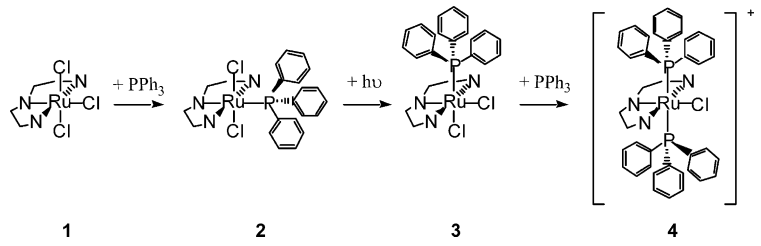

Scheme 1.

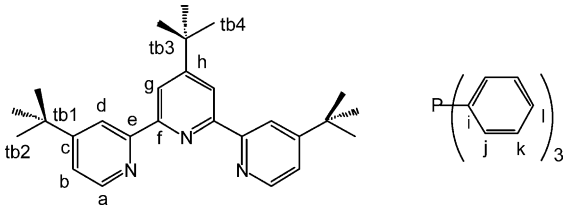

Scheme 2.

Interestingly, a comparison of the electronic spectra of **4** and **4′** indicates no significant differences in the energies of the absorbance bands, i.e., the λ_{max} of the MLCT band for both the trpy* and trpy complexes is 473 nm even though the $E_{1/2}$ value of the trpy* complex **4** is 90 mV lower than that of the trpy complex **4′**. The inconsistency in the differences between the trpy and trpy* absorption maxima and $E_{1/2}$ values may indicate that multiple electronic transitions are involved and, as stated above, the visible absorbances actually reflect a manifold of transitions with slightly different energies due to the geometries of the particular complexes.

3.3. Electrochemistry

Cyclic voltammetry was used to measure the redox potentials and reversibilities of the (trpy*)ruthenium complexes in non-aqueous media. The $E_{1/2}$ values for the quasi-reversible Ru(III/II) couples are summarized in Table 1. For the trpy* complexes, the Ru(III/II) potential for **3** is 120 mV more positive than that for **2**, an effect that has been observed for other *trans–cis* pairs [21,23,24,27–29]. The addition of a second triphenylphosphine ligand to complex **3** (to produce complex **4**) increases the $E_{1/2}$ values by an additional 260 mV, consistent with other *trans*-(diphosphine)ruthenium complexes [23,24,27–29].

Hadda and Le Bozec [19,20] reported that the presence of the *tert*-butyl substituents enhanced the electron-donating influence of the trpy ligand when $[Ru(bpy)Cl(trpy)]^+$ was compared to $[Ru(bpy^*)Cl(trpy^*)]^+$. They observed a decrease in the potential of the Ru(III)/(II) couple of approximately 75 mV when both trpy* and bpy* were substituted for trpy and bpy, respectively. We have observed both smaller (40 mV for **2** vs. **2′** and **3** vs. **3′**) and larger (100 mV for **4** vs. **4′**) changes in the Ru(III/II) redox potentials when trpy* was substituted for trpy in ruthenium(II) complexes. While it is expected that the electron-donating ability of the trpy* ligand is constant in each of the complexes, the potentials of these complexes **2**–**4** may also be affected by the steric size of the trpy* ligand. The size of spectator ligands has been observed to effect the redox potential of the metal center in several examples in the literature [22b,30]. The importance of the steric

Table 1
Electronic spectroscopy and electrochemical data for ruthenium(trpy) and (trpy*) complexes

Complex	$E_{1/2}$ (V) (ΔE_p, mV) [a]	λ_{max}, nm (10^{-3} ε, M^{-1} cm^{-1})
trans-$[RuCl_2(trpy)(PPh_3)]$ (**2′**)	+0.46 (70) [b,c,d]	705 (sh), 549 (4.66), 403 (4.71), 375 (sh), 331 (17.9), 320 (sh), 286 (sh), 275 (16.5) [b,e]
trans-$[RuCl_2(trpy^*)(PPh_3)]$ (**2**)	+0.42 (90) [b]; +0.41 [b,f]	694 (sh), 542 (4.5), 404 (5.3), 328 (21.9), 319 (sh) [b]
cis-$[RuCl_2(trpy)(PPh_3)]$ (**3′**)	+0.58 (65) [b,c,d]	531 (4.79), 488 (sh), 363 (sh), 319 (20.8), 286 (sh), 275 (16.3) [b,e]
cis-$[RuCl_2(trpy^*)(PPh_3)]$ (**3**)	+0.54 (130) [b]; +0.55 [b,f]	524 (5.2), 497 (sh), 356 (sh), 313 (25.0), 290 (sh), 277 (26.3) [b]
trans-$[RuCl(trpy)(PPh_3)_2][PF_6]$ (**4′**)	+0.89 (70) [c,d,g]	473 (3.62), 431 (sh), 330 (sh), 312 (23.2), 268 (43.2) [g]
trans-$[RuCl(trpy^*)(PPh_3)_2][PF_6]$ (**4**)	+0.80 (60) [g]	473 (4.7), 436 (sh), 328 (sh), 311 (30.5), 269 (48.2), 231 (sh) [g]

[a] Unless otherwise noted, half-wave potentials ($E_{1/2} = E_{p,anodic} + E_{p,cathodic}/2$) were measured from cyclic voltammograms vs. an SSCE reference electrode with Pt working and auxiliary electrodes. Data were recorded at 100 mV s^{-1} in 0.1 M Bu_4NBF_4 and referenced vs. internal ferrocene. $\Delta E_p = |E_{p,c} - E_{p,a}|$.

[b] Recorded in CH_2Cl_2.

[c] Reported in Ref. [27].

[d] $E_{1/2}$ vs. SSCE in 0.1 M Bu_4NPF_6 at 200 mV s^{-1} with a Pt working electrode.

[e] Reported in Ref. [23].

[f] Reported in Ref. [21]; $E_{1/2}$ vs. unreported reference, in 0.1 M Bu_4NPF_6 at 200 mV s^{-1} with a Pt working electrode.

[g] Recorded in CH_3CN.

influence of the trpy* ligand was further corroborated by the differences in peak potentials ($\Delta E_p = |E_{p,c} - E_{p,a}|$). For the trpy* complexes, the ΔE_p values of 60–130 mV were, in general, more variable and considerably larger than those of the analogous trpy complexes ($\Delta E_p = 65–70$ mV). This increase in ΔE_p is indicative of greater electrochemical irreversibility in the trpy* complexes. Such irreversibility may be due to the difficulty of the trpy* complexes to compensate (in terms of changing bond lengths and angles), when the complexes are oxidized and/or reduced. This difficulty may be due to the steric strain induced by the interaction of the *t*-butyl groups of the trpy* ligand and the phenyl rings of the PPh_3 ligand(s). This is further discussed during the examination of the X-ray crystal structures of **3** and **4**.

3.4. NMR spectroscopy

^1H, ^{13}C and ^{31}P NMR spectroscopies were used to confirm the structures and investigate the effects of changes in geometry of the low spin, d^6, (trpy*)ruthenium(II) complexes. Scheme 2 gives the designations used in the discussion of the NMR assignments; Table 2 contains ^1H NMR assignments (chemical shifts and coupling constants) and Table 3 contains ^{13}C and ^{31}P NMR assignments.

3.4.1. Analyses of the free trpy* spectra

We have previously discussed revised NMR spectral assignments for the uncoordinated trpy ligand [23] and the ^1H NMR spectrum for the uncoordinated trpy* ligand has been reported by Ben Hadda and Le Bozec [19] in CD_3Cl. Herein, we report the ^1H NMR spectrum of trpy* (taken in CH_2Cl_2 for easier comparison with our ruthenium complex spectra) as well as the ^{13}C NMR spectrum of the uncoordinated trpy* ligand (which has not previously been reported).

In analogy to trpy, the uncoordinated trpy* contains terminal pyridine rings which are magnetically equivalent. Uncoordinated trpy* is also expected to demonstrate a *trans*,*trans*-configuration in solution due to the repulsion of the non-bonding electrons on the nitrogen atoms. The proton–proton coupling constants (e.g., J_{ab}, J_{ac} and J_{bd}) were used to confirm the proton assignments in many of the reported ruthenium complexes. The protonated carbons of the ^{13}C NMR spectrum were assigned from HETCOR analysis. Carbons c and d are of the correct height and in the proper region of the spectrum as predicted by the ChemWindow 3 C-13 NMR Module [25]. Carbons e and f are in the correct region; however, their individual shifts may be switched since their values are close and both carbons have the same intensity (as expected).

3.4.2. Analyses of triphenylphosphine spectra

The ^1H NMR spectrum of free triphenylphosphine (PPh_3) shows one broad singlet in the aromatic region at δ 7.28 ppm in $CDCl_3$ [31]. The ^{13}C NMR spectrum of PPh_3 shows seven peaks at δ 137.27, 137.12, 133.79, 133.53, 128.60, 128.44, and 128.35 ppm in $CDCl_3$ [31]. NMR studies have been successful in characterizing the

Table 2
^1H NMR chemical shifts for the uncoordinated trpy* ligand and the ruthenium(trpy*) and trpy complexes

^1H chemical shifts	trpy*					trpy		
	Ligand	Fresh **2**	Aged **2**	**3**	**4**	**2′**	**3′**	**4′** [a]
A	8.586	8.019	8.110	9.106	8.808	8.286	9.270	9.009
B	7.353	6.856	6.861	7.333	7.080	6.926	7.338	7.107
C	–	–	–	–	–	7.662	7.666	7.687
D	8.756	7.976	7.992	7.707	7.505	8.066	7.746	7.745
G	8.481	8.057	8.108	7.627	7.415	8.153	7.561	7.469
H	–	–	–	–	–	7.901	7.402	7.469
J	–	7.775	7.787	7.198	7.056	7.836	7.227	7.135
K	–	7.250	7.255	7.052	7.038	7.320	7.055	7.075
L	–	7.304	7.305	7.182	7.229	7.375	7.179	7.243
Tb2	1.426	1.293	1.296	1.375	1.302	–	–	–
Tb4	1.454	1.506	1.514	1.470	1.480	–	–	–
J_{ab}	5.3	6.0	6.1	6.0	6.0	5.8	5.4	5.4
J_{ac}	–	–	–	–	–	1.7	1.5	1.3
J_{ad}	0.7	nd[b]	nd	0.5	nd	0.7	0.6	Nd
J_{bc}	–	–	–	–	–	7.6	7.4	7.4
J_{bd}	2.1	2.2	2.2	2.1	1.8	1.4	1.5	1.6
J_{cd}	–	–	–	–	–	8.1	8.1	8.3
J_{gh}	–	–	–	–	–	8.0	8.0	[c]

[a] NMR spectrum has been previously reported in Ref. [23].
[b] nd, not determined.
[c] Protons g and h are magnetically equivalent; the coupling constant cannot be determined.

Table 3
^{13}C and ^{31}P NMR chemical shifts for the uncoordinated trpy* ligand and the ruthenium(trpy*) and trpy complexes

	trpy*					trpy		
^{13}C chemical shifts	ligand	fresh **2**	aged **2**	**3**	**4**	**2′**	**3′**	**4′** [a]
a	149.10	158.02	158.04	154.36	155.14	157.86	154.36	155.79
b	121.15	122.55	122.82	124.00	124.31	124.93	126.26	126.84
c	160.85	157.93	nd [b]	160.09	161.81	135.40	135.09	136.87
d	118.45	119.64	119.88	118.55	119.04	122.27	121.26	122.66
e	156.46	160.75	nd	159.00	157.68	nd	159.47	158.18
f	155.51	160.63	nd	155.43	157.25	nd	158.58	157.66
g	117.92	118.26	118.17	118.39	119.44	120.48	120.77	122.83
h	162.18	159.59	nd	159.68	157.77	131.05	129.82	132.52
i	–	nd	135.91	133.08	130.82	nd	131.69	130.13
j	–	135.57	135.56	133.22	133.30	135.09	132.62	133.23
k	–	127.99	127.91	127.93	128.37	127.64	127.67	128.57
l	–	129.43	129.41	129.11	129.87	129.17	128.91	130.10
tb1	35.28	35.09	35.12	35.32	35.39	–	–	–
tb2	30.66	30.70	30.61	30.65	30.50	–	–	
tb3	35.59	35.97	35.94	35.65	35.83	–	–	–
tb4	30.87	31.00	30.98	31.09	31.21	–	–	–
$^{1}J_{PC}$	–	nd	~32 [c]	42.0	39.2	nd	41.9	39.2
$^{2}J_{PC}$	–	nd	10.1	9.5	10.3	8.2	9.4	10.3
$^{3}J_{PC}$	–	nd	8.5	9.2	9.0	6.5	9.2	9.1
$^{4}J_{PC}$	–	nd	~0	2.2	~0	~0	2.3	1.6
^{31}P chemical shifts	–	~45	46.04	44.20	22.66	44.20 [d]	41.1	21.10

[a] For **4** and **4′**, the $|^{i}J_{PC}|$ coupling is actually $|^{i}J_{PC}+^{j}J_{PC}|$ where $j=i+2$.
[b] nd, not determined.
[c] Unreliable values were obtained due to line broadening.
[d] Aged sample had a ^{31}P NMR chemical shift of 44.20 ppm with a $J_{PC}=37$ Hz.

dynamic processes of PPh_3 ligands in many transition metal complexes [32,33]. Rotation about the three P–C_{ipso} bonds as well as the metal–P bond is possible. Brock and Ibers [34] have estimated these barriers to rotation to be less than 2 kcal mol^{-1}. For steric reasons, the three phenyl groups generally adopt a chiral propeller-like conformation (with either a clockwise or counter-clockwise screw configuration) and this is observed in the crystal structures of **3** and **4** (vide infra) [33]. The interconversion of the two enantiometric configurations or full rotation about any P–C_{ipso} bond requires cooperative motion within the PPh_3 [34].

3.4.3. Analyses of the ruthenium complex spectra

The literature contains very little NMR spectral data on the differences between *trans*- and *cis*-[$RuCl_2$(trpy or trpy*)(PR_3)] complexes, even though these complexes are diamagnetic, monomeric, and highly soluble in a variety of common NMR solvents [21,26]. We herein report the NMR comparison of the trpy* and analogous trpy (**2′**–**4′**) ruthenium complexes.

Interestingly, there are subtle changes in ^{1}H NMR shifts of the trpy* protons of **2** when fresh (observed immediately after purification) and aged (left in CD_2Cl_2, in the dark, for 1–2 days) samples are compared in CD_2Cl_2 (see Table 2). These differences can be significant as demonstrated by chemical shifts of H_a and H_g which increased by 0.091 and 0.051 ppm on aging, respectively. The chemical shifts due to the aging of **2** are much larger for the trpy* pyridyl rings than for the PPh_3 groups (maximum chemical shift difference on aging was 0.012 ppm) or the *t*-butyl groups of the trpy* ligand (maximum difference on aging was 0.008 ppm). At this point, we cannot explain the cause of the shifts caused by the aging of **2**. It should be noted, however, that the chemical reactivity of **2** did not change with aging (i.e., both fresh and aged samples of **2** converted to **3** with similar yields and purities) and the chemical shift differences between the fresh and aged samples of **2** are significantly smaller than the chemical shift differences found between the isomers (e.g., **2** vs. **3** or **4**). Additionally, chemical shift differences were not observed with fresh and aged samples of **3** or **4**, nor where they observed for any of the trpy analogues (**2′**–**4′**). The ^{13}C NMR shifts did show some changes between aged and fresh samples of **2**; however, these differences in chemical shift are not as significant as those found in the ^{1}H NMR spectra. The largest differences in **2** on aging occur with C_b and C_d which shift downfield by 0.27 and 0.24 ppm, respectively. Notably, while others have reported the ^{1}H NMR spectrum of **2** and **3**, no mention was made of the instability in the NMR spectrum of **2** with time. For the rest of our discussion, we will make comparisons based on fresh samples of **2** only.

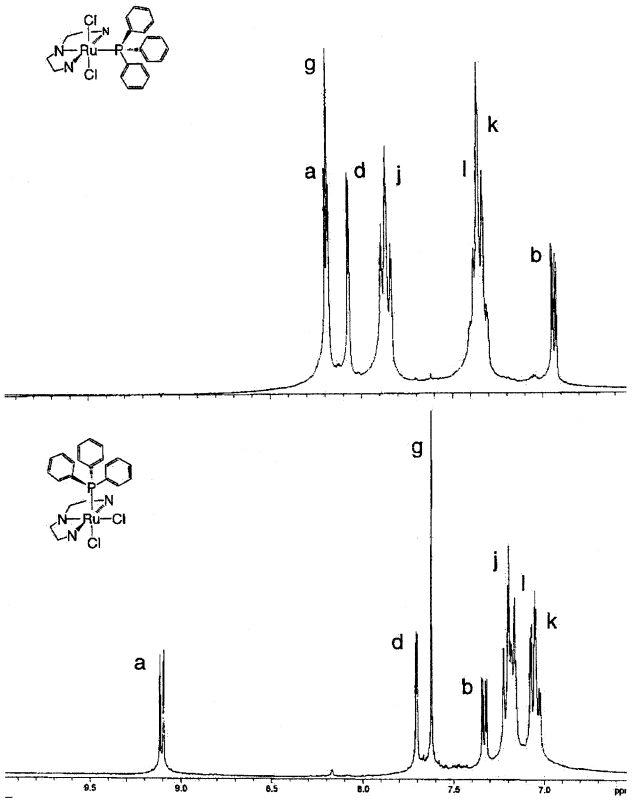

Fig. 1. Proton NMR spectra (400 MHz, CD_2Cl_2) of (a) a fresh sample of *trans*-[$RuCl_2$(trpy*)(PPh_3)] (**2**) and (b) *cis*-[$RuCl_2$(trpy*)(PPh_3)]. The proton assignments are the same as that of Scheme 2.

Fig. 1 compares the aromatic region of the ^1H NMR spectrum of a freshly prepared sample of **2** with the same region of **3**. The proton shifts in these ruthenium complexes clearly reflect the position of the triphenylphosphine ligand(s) relative to the meridional trpy or trpy* ligands. For example, the shift for the H_a protons in **2** (or **2′**) are 1.09 (0.98) ppm upfield of those in **3** (**3′**) and 0.79 (0.72) ppm upfield of that in **4** (**4′**). Other protons show similar, though slightly less dramatic, trends: the H_b of trpy* (trpy) demonstrates a downfield shift of 0.48 (0.41) ppm on going from **2** (**2′**) to **3** (**3′**) and 0.22 (0.18) ppm on going from **2** (**2′**) to **4** (**4′**). In addition to changes in the ^1H spectra of the trpy* and trpy ligands on change in geometry, the triphenylphosphine ligand(s) also shows significant changes in their chemical shifts when the geometry about the ruthenium center is altered. The H_j of trpy* (trpy) demonstrates a upfield shift of 0.58 (0.61) ppm on going from **2** (**2′**) to **3** (**3′**) and 0.72 (0.70) ppm on going from **2** (**2′**) to **4** (**4′**). These differences clearly delineate the position of the triphenylphosphine ligand as being either in the same plane as the terpyridyl ligand (lower H_a, higher H_b and H_j chemical shifts) or perpendicular to the terpyridyl ligand (higher H_a and H_b and lower H_j chemical shifts).

When the proton chemical shifts of the triphenylphosphine ligand are compared to the uncoordinated PPh_3 ligand, the chemical shifts in **2** and **2′** show downfield shifts in the PPh_3 resonances when the chemical shifts in the complexes are compared to those of free PPh_3. For complexes **3** and **4**, the PPh_3 resonances are 0.05–0.24 ppm upfield of their expected position and for the analogous trpy compounds these shifts were observed 0.04–0.21 ppm upfield. These shifts have been attributed to a mutual anisotropic deshielding between the phenyl rings of the PPh_3 ligand and the trpy ligand [23]. As only three chemical shifts are observed for the PPh_3 ligand(s) of **2**–**4**, free rotations about all three P–C_{ipso} bonds as well as those of the Ru–P bonds are indicated. Notably, the ORTEP diagrams of **3** and **4** (Figs. 2 and 3, respectively) show that (a) each phenyl group of the PPh_3 ligands has a slightly different orientation depending on its position relative to the trpy* ligand and (b) the PPh_3 ligands in **3** and **4** are similarly arranged regardless of whether there is one or two PPh_3 ligands in the complex. In each structure, two of the phenyl rings of each PPh_3 ligand are located in an approximately parallel arrangement to the trpy* ligand and the third phenyl ring is nearly perpendicular to the plane of the terminal trpy* pyridines. From the NMR data and the X-ray structures of **3** and **4**, it is postulated that as the PPh_3 ligand(s) rotates along the Ru–P bond, each phenyl ring adjusts its orientation along the P–C_{ipso} axis. That is, as each phenyl ring moves around the Ru–P bond, it may travel in a monotonic or slightly oscillatory path over the trpy* ring, but as it clears the

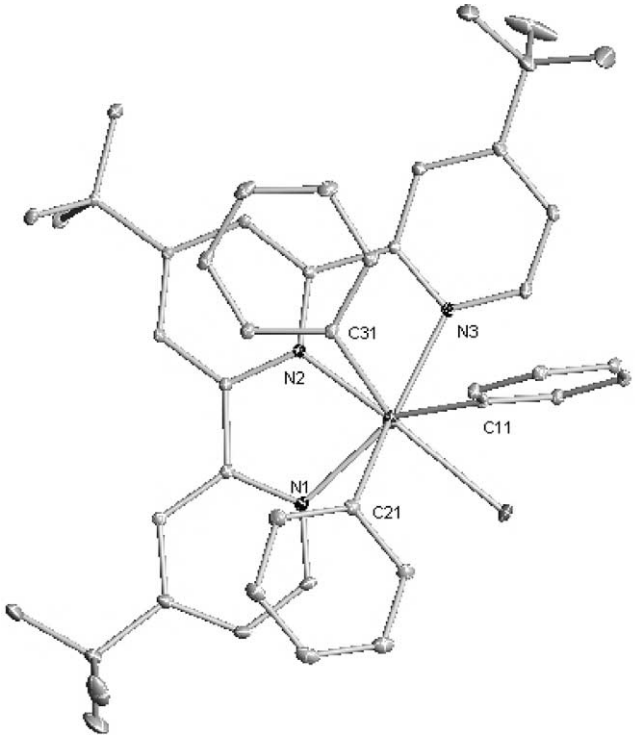

Fig. 2. ORTEP diagram of *cis*-[$RuCl_2$(trpy*)(PPh_3)] (**3**) viewed down the P(1)–Ru–Cl(2) axis (drawn at 10% probability).

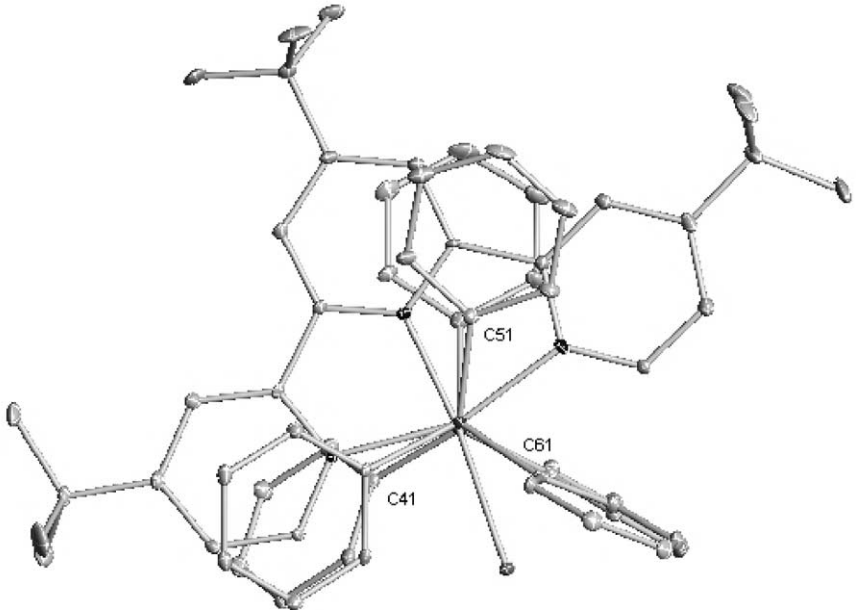

Fig. 3. ORTEP diagram of *trans*-$[RuCl(trpy^*)(PPh_3)_2]^+$ cation (**4**) viewed down the P(2)–Ru–P(1) axis (drawn at 10% probability).

plane above (and/or below) the trpy* ligand, the phenyl rings may rotate about the P–C_{ipso} bonds to become perpendicular to the trpy* ring. This rotation causes time averaging of the *ortho* and *meta* proton resonances and results in only three unique proton resonances for the PPh_3-phenyl rings. Notably, the bulky *t*-butyl groups of the trpy* ligand do not sterically hinder of the motion of the PPh_3 ligand(s) in either **3** or **4**. Finally, while we have not been able to grow X-ray quality crystals of **2**, the NMR spectrum of this complexes indicates that even the positioning of the PPh_3 ligand in the same plane as the trpy* ligand does not hinder the rotation of the Ru–P or P–C_{ipso} groups.

If the rotations of the Ru–P and P–C_{ipso} bond freely occur, the chemical shifts of the PPh_3 ligands are expected to be upfield relative to the free PPh_3 ligand, since the PPh_3 ligands of **3** and **4** spend more time in the shielding areas over the trpy* compared to the two pockets between the chlorine and each of the terminal pyridines of trpy* ligand. Similarly, the trpy* protons (except H_a) should experience shielding by the phenyl rings of the PPh_3 ligands and should be found upfield when compared to the free trpy* ligand. As these general upfield shifts are indeed observed in both the PPh_3 and trpy* ligands, anisotropic deshielding may be the cause. Notably, the H_a protons are expected to be unique since the phenyl rings of the PPh_3 may freely rotate once they clear the plane of the trpy* ligand. The downfield shift for H_a of **3** and **4** may be due to the anisotropic deshielding from the phenyls in the pockets.

Finally, it has been observed that the two *trans*-triphenylphosphine ligands of **4** deshield the trpy* protons somewhat less than the one triphenylphosphine of **3**. This may be due, in part, to the slightly different cogging mechanisms of the phenyl rings when undergoing concerted or unconcerted motions. While the proton shifts are very sensitive to the relative orientation of the trpy* ligand and the phenyl rings of the phosphine(s), the protons do screen the carbons nuclei. The chemical shifts in ^{13}C NMR spectra are less sensitive to the changing geometries about ruthenium center (see Table 3). A comparison of the carbon chemical shifts shows that the C_a of both the trpy and trpy* complexes has greater shielding (occurs at higher frequency) when the triphenylphosphine is moved from the meridional position in the **2** or **2′** isomer to the axial position in the other **3** (**3′**) or **4** (**4′**).

The triphenylphosphine ligands in the ^{13}C NMR spectrum of **4** are observed as a set of four triplets. The signals are triplets due to virtual coupling to the second phosphorus nuclei. Since the two-bond P–Ru–P′ coupling is much larger than the P–C couplings, the higher-order pattern is a triplet rather than a doublet-of-doublets or a pentuplet as only the algebraic sum of the two P–C couplings can be measured across the outer line of the triplet. For **4**, the coupling constant values are $ipso = |^1J_{P-Ci} + {}^3J_{P-Ci}| = 39.2$ Hz, $ortho = |^2J_{P-Cj} + {}^4J_{P-Cj}| = 10.3$ Hz, $meta = |^3J_{P-Ck} + {}^5J_{P-Ck}| = 9.0$ Hz, and $para = |^4J_{P-Cl} + {}^6J_{P-Cl}| = 0$ Hz. These values are nearly the same as those that were observed for the analogous trpy complex except that in **4′** we were able to measure the *para* coupling at 1.6 Hz [23]. Finally, there were no important changes in the J_{P-C} for phenyl carbons with structural position (meridional or axial relative to trpy*) but, for a given complex, the value for the *meta* carbon is always smaller than the *ortho* carbon value. This observation allowed for the absolute assign-

ment of phenyl protons via a carbon–proton HETCOR experiment.

Freshly prepared samples of *trans*-[$RuCl_2$(trpy*)(PPh_3)] had ^{31}P NMR chemical shifts of about 45 ppm with linewidths up to 1000 Hz (see Table 3). After sitting for a day or two, the linewidth decreased to 10 Hz and the chemical shift increased to 46.04 ppm. While this shift compares well to the reported value of 46.45 ppm in the literature [21], there is no previous mention of the initial wide line nor the decrease in linewidth when the complex ages in CD_2Cl_2. Again, we presently have no explanation for this behavior. Interestingly, **2′** had a line width of 48 Hz when freshly prepared but this decreased to 37 Hz after 3 days and did not change thereafter. The chemical shift of **2′** (44.66 ppm) did not change with aging.

Our ^{31}P NMR chemical shift of 44.20 ppm for **3** in CD_2Cl_2 is similar to the 44.59 ppm value of Le Bozec and coworkers [21]. The linewidth for **3** was typically 17 Hz and did not change over time. The corresponding trpy complex **3′** had a chemical shift of 41.1 ppm and a linewidth of 1.5 Hz. When a second triphenylphosphine is added to **3** or **3′** to form **4** or **4′**, the ^{31}P NMR chemical shifts decrease to 22.66 and 21.21 ppm, respectively.

We note that Meyer and coworkers [27] found a large shift difference for the *trans*- and *cis*-[$RuCl_2$(trpy)(P(*p*-$C_6H_4CH_3)_3$)] isomers in CH_3CN (referenced to 15% H_3PO_4 in D_2O). They reported chemical shifts of 27.3 and 41.6 ppm, respectively. We suspect that the literature value of their *trans*-[$RuCl_2$(trpy)(P(*p*-$C_6H_4CH_3)_3$)] complex may be in error.

3.5. X-ray structural analyses

The molecular structures of **3** and **4** have been established by X-ray crystallography (Figs. 4 and 5). The crystal and structure refinement data are summarized in Table 4 and selected bond angles and lengths are listed in Tables 5 and 6 for complexes **3** and **4**, respectively. Crystals of **3** and **4** were grown using the double vial diffusion technique in CH_2Cl_2–toluene solutions. While complex **3** crystallized in a molecular unit, the overall structure of complex **4** consists of an array of ordered ruthenium cations and anions (PF_6^-) in a 1:1 stoichiometry along with solvent of crystallization.

Compound **3** co-crystallized with one-half of a molecule of dichloromethane and one molecule of toluene in the unit cell. The dichloromethane was both positionally and occupationally disordered while the toluene was positionally disordered in the unit cell. Squeeze/Platon [35] was applied to resolve the disordered solvent. Within the 1345.5 $Å^3$ of void space accessible to the solvent molecules, a total of 239 electrons were calculated, compared to the 284 electrons predicted for the presence of two molecules of methylene chloride and four molecules of toluene. It should be noted that in this treatment, the contribution of the solvent molecules is collective and not as individual atoms. Hence, the atom list does not contain the atoms of the solvent molecules.

Compound **4** co-crystallized with a molecule of methylene chloride disordered in the unit cell. Again, Squeeze/Platon [35] was applied to resolve the disordered solvent. Within the 804.5 $Å^3$ of void space accessible to solvent molecules, a total of 175 electrons were calculated, compared to 168 electrons predicted for the presence of four molecules of methylene chloride.

The ruthenium atoms in each structure reside in a distorted octahedral environment with a trpy* bite angle, N(1)–Ru–N(3), of 159.44(6)° and 157.9(2)° for complexes **3** and **4**, respectively. These bite angles are consistent with those found for other (trpy)ruthenium complexes, namely *trans*-[$RuCl$(trpy)($PPh_3)_2$](BF_4), 157.9(3)° [23], *trans*-[$Ru(NO_2)$(trpy)($PMe_3)_2$](ClO_4), 158.3(2)° [36], *trans*-[$Ru(H_2O)$(trpy)($PEt_3)_2$]($ClO_4)_2$, 158.3(3)° [37], and *trans*-[$Ru(NO_2)$(trpy)($PPh_3)_2$](PF_6), 156.9(5)° [38]. The deviations from the ideallized 180° attributed to an octahedral geometry are similar to those that have been observed for trpy and are attributed to the geometrical constraints of the trpy* backbone. The Ru–N(*i*) ($i = 1$–3) bond lengths range from 1.9418(15) to 2.0702(17) Å in **3** and 1.957(5) to 2.094(4) Å in **4** with the shortest Ru–N bond distance in both complexes between the ruthenium and the nitrogen of the central pyridine ring of trpy. Asymmetric bond lengths exist between the ruthenium center and terminal nitrogens of the trpy* ligand in both **3** and **4**; however, all these Ru–N bond distances are typical of other (trpy)ruthenium complexes: 1.952(9)–2.098(6) [36–39].

For complex **4**, the P(1)–Ru–P(2) bond angle of 177.73(6)° also deviates slightly from linearity (180°). A normal range for *trans*-(P–Ru–P) angles is given as 175.1(1)° to 178.2(2)° for PMe_3 [36], PEt_3 [37], PPr_3 [39], and PPh_3 [23,40] complexes. Notably, the P–Ru–P bond axis appears to bend in the direction of the chloride ligand, implying that this region is less sterically crowded than the region around the trpy* ligand.

A comparison of the ORTEP representations of **3** and **4** (Figs. 2 and 3, respectively) indicates that the phenyl rings of the triphenylphosphine ligand(s) align in similar positions about the trpy* ligand regardless of whether one or two PPh_3 ligands is coordinated to the ruthenium center. By defining a reference plane for **3** as the plane of the trpy* backbone (N1, N2 and N3), the ruthenium atom and meridional chloride atom, we have examined the angle that the plane of the phenyl rings of PPh_3 make with this reference. The planes containing each of the phenyl rings of the triphenylphosphine ligands are described by the phosphorous atom, the *ipso*-carbon atom of the phenyl ring as well as the adjacent (*ortho*) carbons of the phenyl ring. Using this scheme, it is

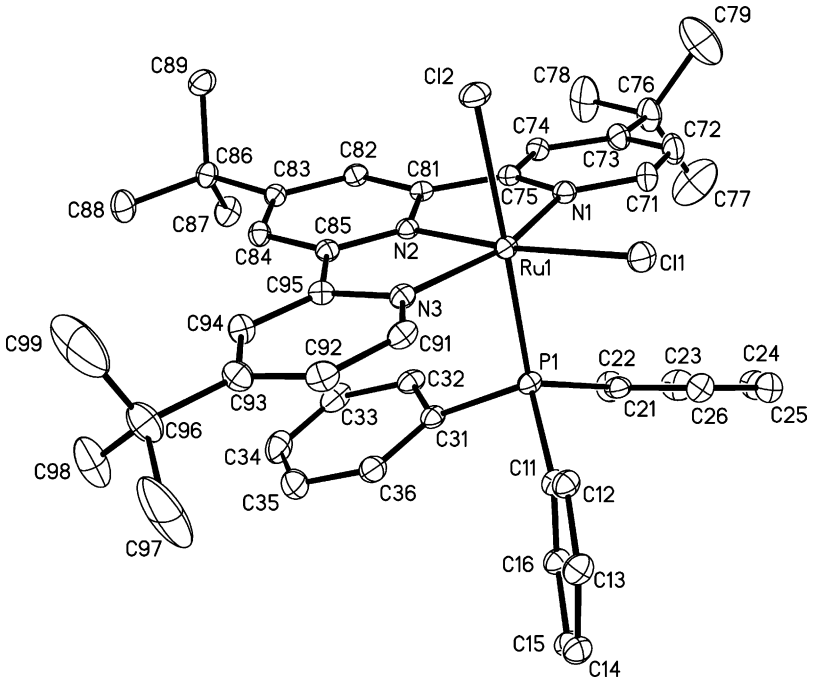

Fig. 4. Molecular structure of *cis*-[Ru(trpy*)(PPh_3)Cl_2] (**3**) (drawn at 30% probability), showing atomic labeling scheme. Hydrogen atoms are omitted for clarity.

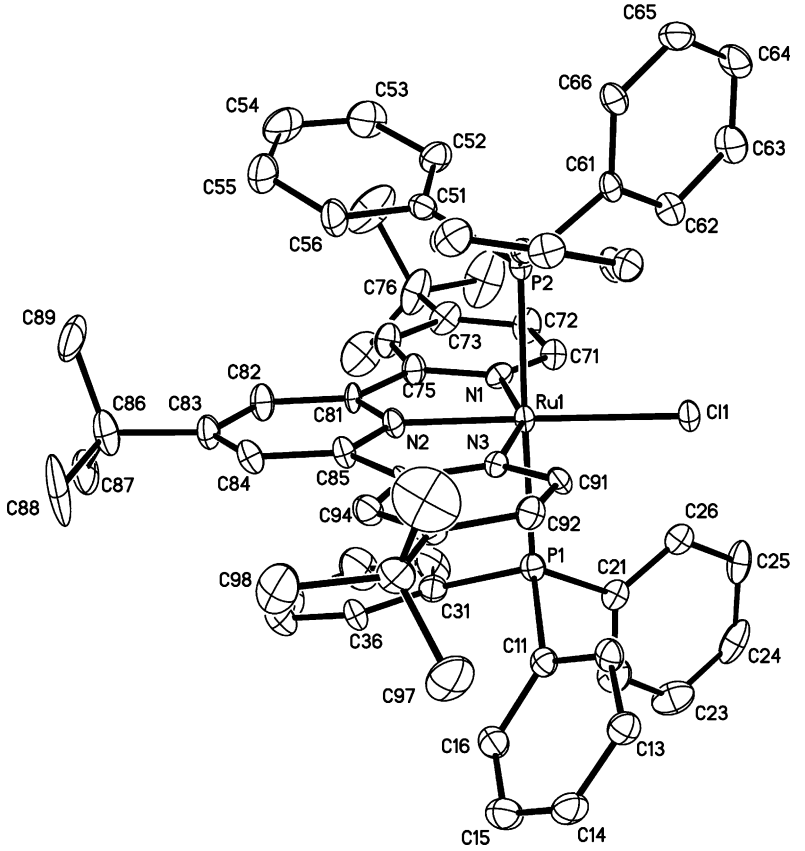

Fig. 5. Molecular structure of *trans*-[Ru(Cl)(trpy*)(PPh_3)$_2$]$^+$ cation (**4**) (drawn at 30% probability), showing labeling scheme. Hydrogen atoms are omitted for clarity.

Table 4
Crystal data and structural refinement for *cis*-[$RuCl_2(trpy^*)(PPh_3)$] (**3**) and *trans*-[$RuCl(trpy^*)(PPh_3)_2]PF_6$ (**4**)

	3	**4**
Empirical formula	$C_{45}H_{50}C_{12}N_3PRu$	$C_{63}H_{65}ClF_6N_3P_3Ru$
Formula weight	835.82	1207.61
Temperature (K)	173(2)	173(2)
Wavelength (Å)	0.71073	0.71073
Crystal system	monoclinic	monoclinic
Space group	$P2_1/c$	$P2_1/n$
Unit cell dimensions		
a (Å)	13.7888(7)	11.9588(7)
b (Å)	24.3826(13)	19.1204(11)
c (Å)	13.4235(7)	28.8601(17)
α (°)	90	90
β (°)	101.9930(10)	92.1080(10)
γ (°)	90	90
V (Å^3)	4414.6(4)	6594.6(7)
Z	4	4
Density (calculated) (Mg m^{-3})	1.258	1.216
Absorption coefficient (mm^{-1})	0.545	0.405
F(0 0 0)	1736	2496
Crystal size (mm^3)	0.60 × 0.40 × 0.40	0.40 × 0.20 × 0.20
Theta range for data collection (°)	1.67–28.30	1.41–25.00
Index ranges	$-16 \le h \le 13$, $-28 \le k \le 31$, $-17 \le l \le 17$	$-13 \le h \le 13$, $-22 \le k \le 22$, $-33 \le l \le 33$
Reflections collected	21 205	26 623
Independent reflections	9260 ($R_{int} = 0.0251$)	10 868 ($R_{int} = 0.0686$)
Completeness to theta	28.30° (84.4%)	25.00° (3.5%)
Absorption correction	semi-empirical/SADABS	semi-empirical/SADABS
Max. and min. transmission	0.8115 and 0.7358	0.9233 and 0.8547
Refinement method	Full-matrix least-squares on F^2	Full-matrix least-squares on F^2
Data/restraints/parameters	9260/0/478	10 868/20/704
Goodness-of-fit on F^2	1.005	1.080
Final R indices [I > 2σ(I)]	$R_1 = 0.0307$, $wR_2 = 0.0859$	$R_1 = 0.0748$, $wR_2 = 0.1712$
R indices (all data)	$R_1 = 0.0362$, $wR_2 = 0.0889$	$R_1 = 0.1177$, $wR_2 = 0.1895$
Largest diff. peak and hole (e Å^{-3})	0.479 and −0.374	1.214 and −0.855

Table 5
Selected bond lengths (Å) and angles (°) for *cis*-[$RuCl_2(trpy^*)(PPh_3)$] (**3**)

Ruthenium–ligand distances			
Ru(1)–N(1)	2.0610(17)	Ru(1)–P(1)	2.2803(4)
Ru(1)–N(2)	1.9418(15)	Ru(1)–Cl(1)	2.4448(5)
Ru(1)–N(3)	2.0702(17)	Ru(1)–Cl(2)	2.4507(5)
Phosphorous–carbon distances			
P(1)–C(11)	1.8310(19)		
P(1)–C(21)	1.837(2)		
P(1)–C(31)	1.836(2)		
Angles around the ruthenium atom			
N(2)–Ru(1)–N(1)	79.74(6)	N(2)–Ru(1)–P(1)	92.70(4)
N(2)–Ru(1)–N(3)	79.75(6)	N(1)–Ru(1)–P(1)	91.32(4)
N(1)–Ru(1)–N(3)	159.44(6)	N(3)–Ru(1)–P(1)	91.06(4)
N(2)–Ru(1)–Cl(1)	174.50(5)	N(2)–Ru(1)–Cl(2)	85.73(4)
N(1)–Ru(1)–Cl(1)	97.63(5)	N(1)–Ru(1)–Cl(2)	88.85(4)
N(3)–Ru(1)–Cl(1)	102.69(4)	N(3)–Ru(1)–Cl(2)	88.20(4)
P(1)–Ru(1)–Cl(1)	92.188(17)	P(1)–Ru(1)–Cl(2)	178.361(19)
Cl(1)–Ru(1)–Cl(2)	89.403(17)		
Angles around the phosphorous atoms			
C(11)–P(1)–C(31)	100.32(9)	C(11)–P(1)–Ru(1)	122.13(6)
C(11)–P(1)–C(21)	99.71(9)	C(31)–P(1)–Ru(1)	109.21(6)
C(31)–P(1)–C(21)	108.82(9)	C(21)–P(1)–Ru(1)	115.13(6)

Symmetry transformations were used to generate equivalent atoms.

Table 6
Selected bond lengths (Å) and angles (°) for *trans*-[$RuCl(trpy^*)(PPh_3)_2]PF_6$ (**4**)

Ruthenium–ligand distances			
Ru(1)–N(1)	2.094(4)	Ru(1)–P(1)	2.4070(19)
Ru(1)–N(2)	1.957(5)	Ru(1)–P(2)	2.3779(18)
Ru(1)–N(3)	2.076(4)	Ru(1)–Cl(1)	2.4507(15)
Phosphorous–carbon distances			
P(1)–C(11)	1.840(6)	P(2)–C(41)	1.831(6)
P(1)–C(21)	1.824(7)	P(2)–C(51)	1.828(7)
P(1)–C(31)	1.837(6)	P(2)–C(61)	1.834(6)
Angles around the ruthenium atom			
P(1)–Ru(1)–P(2)	177.73(6)	P(1)–Ru(1)–Cl(1)	90.51(6)
P(2)–Ru(1)–Cl(1)	88.17(6)	P(1)–Ru(1)–N(1)	89.48(15)
P(2)–Ru(1)–N(1)	89.15(15)	Cl(1)–Ru(1)–N(1)	107.43(15)
P(1)–Ru(1)–N(2)	91.05(16)	P(2)–Ru(1)–N(2)	90.48(16)
Cl(1)–Ru(1)–N(2)	173.31(14)	N(1)–Ru(1)–N(2)	79.1(2)
P(1)–Ru(1)–N(3)	92.14(14)	P(2)–Ru(1)–N(3)	89.81(14)
Cl(1)–Ru(1)–N(3)	94.62(13)	N(1)–Ru(1)–N(3)	157.9(2)
N(2)–Ru(1)–N(3)	78.82(19)		
Angles around the phosphorous atoms			
Ru(1)–P(1)–C(11)	116.9(2)	C(11)–P(1)–C(21)	101.0(3)
Ru(1)–P(1)–C(21)	120.9(2)	C(11)–P(1)–C(31)	105.2(3)
Ru(1)–P(1)–C(31)	108.7(2)	C(21)–P(1)–C(31)	102.1(3)
Ru(1)–P(2)–C(41)	111.9(2)	C(41)–P(2)–C(51)	109.6(3)
Ru(1)–P(2)–C(51)	112.2(2)	C(41)–P(2)–C(61)	100.1(3)
Ru(1)–P(2)–C(61)	121.2(2)	C(51)–P(2)–C(61)	100.5(3)

observed that the three phenyl rings on P of complex **3** are oriented at angles of 85.54(0.07)°, 27.78(0.09)° and 18.48(0.06)° from the reference plane (for *ipso*-carbons from C(11) and proceeding clockwise about the P atom). By defining similar reference and phenyl ring planes, we have observed that the three phenyl rings on P(1) of **4** are oriented at angles of 85.54(0.22)°, 16.36(0.14)° and 50.86(0.19)°, 16.36(0.14)° (from *ipso*-carbon C(21) and proceeding clockwise around the P(1) atom) and the three rings on P(2) are oriented at angles of 79.16(0.18)°, 23.68(0.14)°, 24.28(0.20)° from the reference plane (for *ipso*-carbon C(61) and proceeding clockwise about the

P(2) atom). Notably, in the structures of both **3** and **4** one of the phenyl rings lies between the chlorine atom and one of the terminal pyridine rings of trpy*. The second of the phenyl rings lies nearly parallel to the reference surface between the central and terminal pyridyl rings of trpy* and the third phenyl ring lies between the other terminal pyridyl ring and the chlorine atom.

For the structure of **4**, the phenyl rings of (C(21) and C(61)), (C(31) and C(51)) and (C(11) and C(41)) exist as nearly eclipsed pairs. Geometric considerations indicate that each of these phenyl rings may be involved in π-stacking with the trpy* ligand as they are within the prescribed approximately 3.6 Å distance [41]. Finally, it is notable that the alignment of the phenyl rings of the PPh_3 ligands is similar in the trpy* complexes to those of the trpy complex, *trans*-[RuCl(trpy)$(PPh_3)_2$]BF_4 [23], indicating that, at least in the solid state, the bulky *t*-butyl groups do not affect the stabilities observed with the π-stacking [41].

4. Conclusion

A comparison of (triphenylphosphine)ruthenium(II) complexes containing trpy and trpy* reveals many similarities in the two ligands. Electronic and ^1H NMR spectra and electrochemical data were found to readily differentiate the *trans*- and *cis*-[RuCl(trpy or trpy*)(PPh_3)] complexes, while the ^{31}P chemical shift differences between the *trans*- and *cis*-[$RuCl_2$(trpy*)(PPh_3)] complexes were not dramatic. X-ray crystal structure analyses confirmed the structures of the *cis*-[$RuCl_2$(trpy*)$(PPh_3)Cl_2$] and *trans*-[RuCl(trpy*)$(PPh_3)_2$]PF_6 complexes and it was observed that similar π-stacking interactions occurred between the phenyl rings and the trpy* ligand in both complexes.

5. Supplementary materials

Additional crystallographic data for complexes **3** and **4** include: complete bond lengths, complete bond angles, atomic coordinates and equivalent isotropic displacement parameters, anisotropic displacement parameters , and H coordinates and isotropic displacement parameters. X-ray crystallographic data have been deposited with the Cambridge Crystallographic Data Center, CCDC Nos. 201423 for **3** and 201422 for **4**. Copies of this information may be obtained free of charge from The Director, CCDC, 12 Union Road, Cambridge, CB2 1EZ, UK (Fax: +44-1223-336-033; email: deposit@ccdc.cam.ac.uk or www: http://www.ccdc.cam.ac.uk).

Acknowledgements

This work was supported by Research Corporation (CC4252). S.B. was funded by a 1997 Villanova University Chemistry Department Summer Research Fellowship. The authors also wish to thank Ms. Pooja Aggarwal for assistance in the synthesis of the ruthenium complexes.

References

[1] E.C. Constable, Adv. Inorg. Chem. Radiochem. 20 (1986) 69.
[2] M. Maestri, N. Armaroli, V. Balzani, E. Constable, A.M.W.C. Thompson, Inorg. Chem. 34 (1995) 2759.
[3] E.C. Constable, M. Neuburger, D.R. Smith, M. Zehnder, Inorg. Chim. Acta 275–276 (1998) 359.
[4] R.-A. Fallahpour, M. Neuburger, M. Zehnder, Polyhedron 18 (1999) 2445.
[5] S. Liu, A.D. Hamilton, Tetrahedron Lett. 38 (1997) 1107.
[6] E.C. Constable, S. Mundwiler, Polyhedron 18 (1999) 2433.
[7] G. Albano, V. Balzani, E.C. Constable, M. Maestri, D.R. Smith, Inorg. Chim. Acta 277 (1998) 225.
[8] K. Hutchison, J.C. Morris, T.A. Nile, J.L. Walsh, D.W. Thompson, J.D. Petersen, J.R. Schoonover, Inorg. Chem. 38 (1999) 2516.
[9] E.C. Constable, C.E. Housecroft, M. Neuburger, A.G. Schneider, M. Zehnder, J. Chem. Soc., Dalton Trans. (1997) 2427.
[10] D.K. Crites, C.T. Cunningham, D.R. McMillin, Inorg. Chim. Acta 273 (1998) 346.
[11] S.-W. Lai, M.C.W. Chan, K.-K. Cheung, C.-M. Che, Inorg. Chem. 38 (1999) 4262.
[12] (a) F. Krohnke, Synthesis (1976) 1.;
(b) K.T. Potts, M.J. Cipullo, P. Ralli, G. Theodoridis, J. Org. Chem. 47 (1982) 3027;
(c) D.L. Jameson, L.E. Guise, Tetrahedron Lett. 32 (1991) 1999.
[13] A.C. Benniston, Tetrahedron Lett. 38 (1997) 8279.
[14] B. Whittle, E.L. Horwood, L.H. Rees, S.R. Batten, J.C. Jeffery, M.D. Ward, Polyhedron 17 (1998) 373.
[15] E.C. Constable, P. Harverson, D.R. Smith, L. Whall, Polyhedron 16 (1997) 3615.
[16] M.A. Halcrow, E.K. Brechin, E.J.L. McInnes, F.E. Mabbs, J.E. Davies, J. Chem. Soc., Dalton Trans. (1998) 2477.
[17] G.D. Storrier, S.B. Cobran, D.C. Craig, J. Chem. Soc., Dalton Trans. (1998) 1351.
[18] P.E. Rosevear, W.H.F. Sasse, J. Heterocyc. Chem. 8 (1971) 483.
[19] T. Ben Hadda, H. Le Bozec, Polyhedron 7 (1988) 575.
[20] T. Ben Hadda, H. Le Bozec, Inorg. Chim. Acta 204 (1993) 103.
[21] T. Ben-Hadda, C. Mountassir, H. Le Bozec, Polyhedron 14 (1995) 953.
[22] (a) C.A. Bessel, R.F. See, D.L. Jameson, M.R. Churchill, K.J. Takeuchi, J. Chem. Soc., Dalton Trans. 10 (1993) 1563;
(b) C.A. Bessel, J.A. Margarucci, J.H. Acquaye, R.S. Rubino, J. Crandall, A.J. Jircitano, K.J. Takeuchi, Inorg. Chem. 32 (1993) 5779;
(c) C.A. Bessel, P. Aggarwal, A.C. Marschilok, K.J. Takeuchi, Chem. Rev. 101 (2001) 1031.
[23] W.J. Perez, C.H. Lake, R.F. See, L.M. Toomey, M.R. Churchill, K.J. Takeuchi, C.P. Radano, W.J. Boyko, C.A. Bessel, J. Chem. Soc., Dalton Trans. (1999) 2281.
[24] R.A. Leising, J.J. Grzybowski, K.J. Takeuchi, Inorg. Chem. 27 (1988) 1020.
[25] ChemWindow 3, V3.1 C-13 NMR Module, SoftShell International, Grand Junction, CO.

[26] B. Siemens, XRD, Madison, WI.
[27] B.P. Sullivan, J.M. Calvert, T.J. Meyer, Inorg. Chem. 19 (1980) 1404.
[28] R.A. Leising, S.A. Kubow, K.J. Takeuchi, Inorg. Chem. 29 (1990) 4569.
[29] R.A. Leising, S.A. Kubow, L.F. Szczepura, K.J. Takeuchi, Inorg. Chim. Acta 245 (1996) 167.
[30] D.A. Bohling, J.F. Evans, K.R. Mann, Inorg. Chem. 21 (1982) 3546.
[31] C.J. Pouchert, J. Behnke, Aldrich Library of ^{13}C and ^{1}H FT NMR Spectra, 1st ed., Vol. 2, Aldrich Chemical Company, Inc., Milwaukee, WI, 1993, p. 1653.
[32] (a) J.W. Faller, B.V. Johnson, J. Organomet. Chem. 96 (1975) 99; (b) J. Vicente, M.-T. Chicote, M.-C. Lagunas, P.J. Johns, B. Ahrens, Inorg. Chem. 36 (1997) 4938; (c) E.E. Wille, D.S. Stephenson, P. Capriel, G. Binsch, J. Am. Chem. Soc. 104 (1982) 405.
[33] S.G. Davies, A.E. Derome, J.P. McNally, J. Am. Chem. Soc. 113 (1991) 2854 (and references therein).
[34] C.P. Brock, J.A. Ibers, Acta Crystallogr., Sect. B 29 (1973) 2426.
[35] A.L. Spek, Acta Crystallogr., Sect. A 46 (1990) C34.
[36] R.A. Leising, S.A. Kubow, M.R. Churchill, L.A. Buttrey, J.W. Ziller, K.J. Takeuchi, Inorg. Chem. 29 (1990) 1306.
[37] H.J. Lawson, T.S. Janik, M.R. Churchill, K.J. Takeuchi, Inorg. Chim. Acta 174 (1990) 197.
[38] M.R. Churchill, L. Krajkowski, L.F. Szczepura, K.J. Takeuchi, J. Chem. Crystallogr. 26 (1996) 853.
[39] M.R. Churchill, L. Krajkowski, L.F. Szczepura, K.J. Takeuchi, J. Chem. Crystallogr. 26 (1996) 543.
[40] L.F. Szczepura, S.A. Kubow, R.A. Leising, W.J. Perez, M.H.V. Huynh, C.H. Lake, D.G. Churchill, M.R. Churchill, K.J. Takeuchi, J. Chem. Soc., Dalton Trans. (1996) 1463.
[41] M.D. Blanchard, R.P. Hughes, T.E. Concolino, A.L. Rheingold, Chem. Mater. 12 (2000) 1604.